University of Zurich[UZH]

Bachelor thesis

Sensitivity of the DARWIN experiment to axions and axion-like particles

Professor	Prof. Dr. Laura Baudis
Supervisor	Dr. Patricia Sanchez
Student	Livio Redard-Jacot

August 18, 2020

Acknowledgements

At this point I would like to thank all those who have supported me in the realisation of this work.
I would like to thank Prof. Dr. Laura Baudis for giving me the opportunity to do this interesting project from which I have learned so much. I gratefully thank Dr. Patricia Sanchez, my supervisor, for her patient, gentle guidance and inspiring, constant encouragement throughout the course of this work. From the beginning, you have supported me with valuable suggestions and allowed me to ask you for advice at any time. Finally, I want to thank the members of the particle astrophysics group at the University of Zurich for giving me an insight into this exciting field of research.

Contents

1 Introduction

During the last century a broad variety of experiments have tried to understand the fundamental nature of dark matter, but so far it remains one of the greatest unsolved puzzles of modern physics. The observed gravitational interactions with ordinary matter provide overwhelming evidence for the existence of dark matter, but its actual composition is still unknown. Cosmological and astrophysical observations show that dark matter is a non-baryonic form of matter that interacts neither electromagnetically nor strongly. It interacts only gravitationally and eventually weakly. This causes great difficulties to explore the phenomena, even though dark matter accounts for a large amount of the matter in the universe. The standard model of cosmology ΛCDM indicates that dark matter contributes 27% to the total amount of energy in the Universe, whereas the baryonic matter only accounts for 5%. The remaining 68% is dark energy that causes the accelerated expansion of the Universe [1].

The most compelling explanation today suggests that dark matter is made of an elementary particle that is not described by the standard model [2]. In this context, there are two candidates in focus that are predicted by theories independently of the dark matter problem: Axions and Weakly Interacting Massive Particles (WIMPs). Many experiments have tried and try to detect these particles through a signal that is produced by an interaction within a target medium. Nevertheless, no sign of a conclusive signal has been observed so far.

To continue with the search, the future DARWIN dark matter experiment will use 40 t of liquid xenon as a target [3]. The detector aims to provide an unprecedented sensitivity to such particles with a low energy threshold and an ultra-low background. At this stage of the DARWIN project, it is crucial to know the expected background spectrum of the detector to differentiate and characterise a detected signal, that could originate from new physics. The background is mainly produced by radioactive decays in the target and the detector materials as well as by cosmic particles that can reach the detector. This work completes the simulation of the background spectrum for the future DARWIN detector and uses the results to determine its sensitivity to axions and axion-like particles.

The thesis is structured as follows: Section 2 gives an overview of the evidence and the search for dark matter and introduces the design and detection principle of DARWIN. The simulation of the background model and the resulting spectra are described in section 3. The calculation of the sensitivity to axions is presented in section 4, followed by a discussion in section 5.

2 Dark Matter search with DARWIN

2.1 Evidence for dark matter

The observation of different astrophysical objects as well as the study of cosmic structures on large scales led to different sources of evidence for dark matter. The most important ones are explained in the following sections.

2.1.1 Rotation curves of galaxies and clusters

In 1933, the first hint for the existence of dark matter appeared in physics. The astronomer Fritz Zwicky noticed in his observation of the Coma cluster a huge discrepancy with his estimations for the mass of the galaxy cluster [4]. He derived the amount of mass in the cluster from the observed velocity dispersion with the help of the virial theorem, which connects the mean kinetic and potential energy. In a second estimation, Zwicky determined the mass through the luminosity of the galaxies in the cluster. He concluded that there was 400 times more gravitational matter than was visible and denoted the invisible matter as dark matter. Physicists at the time were not sure if this discrepancy could be explained by the discovery of more visible mass in the cosmic structure by using more advanced instruments. Years later X-ray telescopes detected the intracluster medium, a tenous plasma consisting mainly of H and He gas which accounts for most of the baryonic matter of a cluster. However, this amount of mass is not enough to explain the whole gravitational mass. Further research only confirmed that the amount of dark matter makes up for a multiple of the ordinary matter in the cluster and that its nature is completely unknown [5].
More than forty years after Zwicky's observation, Vera Rubin *et al.* provided strong evidence by publishing the measurements of the rotation curves of 21 spiral galaxies [6]. However, the first hint from spiral galaxies had been observed already in 1970 [7]. Figure 1 shows an example of such a rotation curve from the galaxy M33.
Rotation curves describe the orbital velocity of stars depending on their distance to the center of the galaxy. Newtonian dynamics relates the orbital velocity to the mass density of the galaxy:

$$v(r) = \sqrt{\frac{GM(r)}{r}} \tag{1}$$

If there were only stars and gas in galaxies, one would expect a decreasing velocity in the outer regions. However, the observed rotation curves of galaxies show a flat

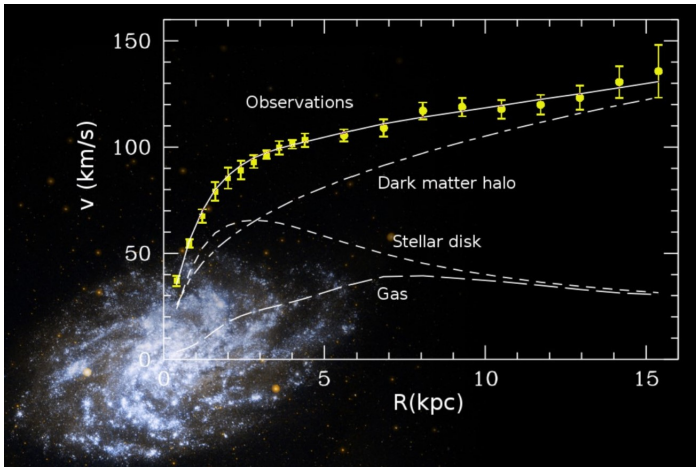

Figure 1: The orbital velocity of the stars in the galaxy M33 as a function of the distance to the galactic center. The observed curve cannot be explained by the mass density of the stars and gas in the galaxy but needs an additional mass. Figure taken from [8].

behaviour or even an increase far away from the center. This behaviour suggests the existence of a dark matter halo in addition to the galaxy's stars, as shown in figure 1. Nowadays precise observation techniques make rotation curves one of the strongest evidence for the existence of dark matter. In addition, these curves also reveal the dark matter distribution in galaxies, including the Milky Way [9].

2.1.2 Gravitational lensing

Gravitational lensing is an alternative way to determine the gravitational mass of large cosmic objects. According to general relativity, light passing by a massive cosmic body between its source and its observer is bent by an angle that depends on the gravitational mass of the body. This effect allows to study the gravitational mass of clusters that have merged and compare it with the visible mass, to show again that dark matter is more abundant than baryonic matter. For the baryonic matter the predominant mass in a merged cluster is the intracluster plasma, that slows down in the collision and is therefore located in the center. On the contrary, gravitational lensing shows that most of the mass can be found in a different location [10]. Figure 2 illustrates an example for the Bullet cluster. The X-ray emission from the intracluster plasma is shown in pink, detected by the Chandra-X-ray satellite, and the total mass distribution in blue, derived through gravitational lensing. The two distributions reveal a large discrepancy.

Figure 2: The merged Bullet cluster. An optical image of the galaxies overlayed with the measurement of the intracluster plasma in pink and the gravitational mass in blue. Figure taken from [11].

2.1.3 Cosmic Microwave Background

Whereas the evidence presented above could possibly be explained with a modified theory of gravity (MOND) [12] or in the case of the merged cluster at least with a smaller amount of dark matter, the cosmic microwave background (CMB) provides strong support for the existence of dark matter [13].
The CMB is a nearly isotropic microwave radiation permeating the entire Universe. Its measurement allows an insight into the formation of the Universe. In the beginning, the Universe was in a hot and dense state, but it cooled down while expanding and became transparent around 380'000 years after the Big Bang. Matter and radiation decoupled and the CMB radiation was released. The temperature spectrum of this radiation is not uniform, but shows extremely small fluctuations (figure 3a). They reveal not only the distribution of matter at this early state of the Universe, but also provide evidence for its composition [14].
Figure 3b shows the CMB power spectrum, that describes the size of the fluctuations depending on the angular scale in the sky. The amplitudes of the peaks allow to determine the entire amount of dark and baryonic matter in the Universe, as well as the dark energy density [2]. The measurements of the CMB by the Planck telescope suggest that the Universe consists of 5% baryonic matter, 27% dark matter and 68% dark energy [16].
Furthermore, a cosmological model that can explain the formation of cosmic structures has been developed, the so-called cosmological standard model ΛCDM [17]. The cosmological parameters derived from the CMB agree very well with the predictions of the ΛCDM model, whereas theoretical models of modified gravity are

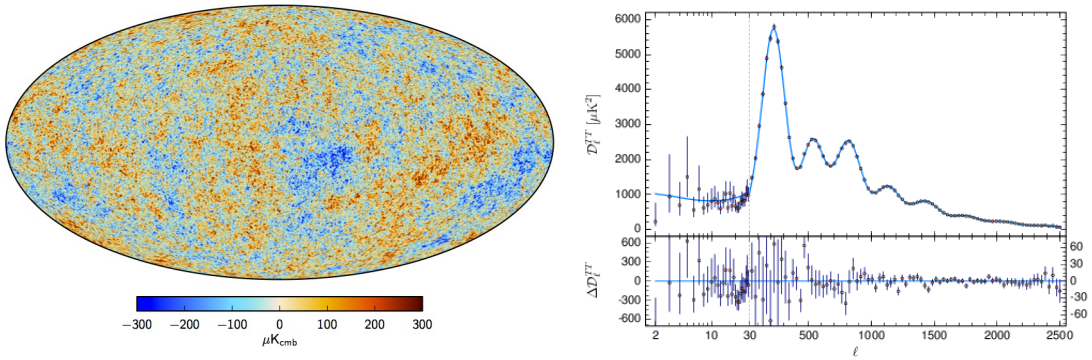

(a) (b)

Figure 3: a) CMB temperature map from the Planck collaboration [15]. b) CMB power spectrum from 2018 with a blue line describing the best-fit of the ΛCDM model [16].

failing here. The success of the ΛCDM model provides therefore strong evidence for dark matter, as it is based on the assumption that the Universe is dominated by non-baryonic dark matter.

2.2 Dark matter candidates

The evidence suggests to look for dark matter in the form of a new particle beyond the standard model. Apart from the gravitational effects of dark matter, little is known about the characteristics of such a particle (assuming it is a particle). Observations from cosmology and astrophysics give certain information: dark matter particles should be stable, or at least have a much longer life span than the age of the Universe. They should interact barely or not at all with the electromagnetic interaction but might interact weakly and they should be non-relativistic [2]. Constraints on the parameter space for the mass and the interaction strength of such particles with standard matter depend on further assumptions but leave a huge range open. The range for dark matter masses spans more than 40 orders of magnitude.
Under this scenario, most of the attention is focused on two types of particles, which were not predicted initially to solve the dark matter problem: Axions and Weakly Interacting Massive Particles (WIMPs). This work will focus on the axions, but will also briefly introduce the WIMPs, since the DARWIN detector is specifically designed to probe these particles.

2.2.1 WIMPs

WIMPs could form the cold dark matter and explain both the formation of the cosmic structures and the observed dark matter density Ω_{DM}. They only interact weakly and gravitationally. They are in the focus of many current and future detection experiments such as DARWIN [3]. Different theories that extend the standard model have predicted such particles. An example is the lightest supersymmetric particle. The theory of Supersymmetry (SUSY) predicts for every bosonic particle of the standard model a fermion and vice versa, a so-called superpartner, and could solve some of the current problems in particle physics such as the *hierarchy problem* [18]. WIMPs could also be the lightest Kaluza-Klein (KK) excitations of standard model particles, introduced in theories of extra dimensional space [19].

2.2.2 Axions and axion-like particles

The axion is another convincing candidate for dark matter. Initially, the axion was a consequence of the Peccei-Quinn solution of the strong CP problem, that arises from the experimentally observed absence of CP violation in the strong interaction. In 1977, Robert Peccei and Helen Quinn presented a natural solution to this problem with a new global U(1) symmetry in the standard model [20]. The spontaneous breaking of this symmetry below an energy scale f_a leads to the prediction of a Nambu-Goldstone boson: the axion [21]. Astrophysical constraints and experimental results have ruled out a symmetry breaking scale around the electroweak scale. Nevertheless, higher symmetry breaking scales still allow the existence of axions, such that they could constitute the dark matter [22]. The symmetry breaking scale f_a is inversely proportional to the axion mass, and further cosmological constraints set the mass of those QCD axions between 1 $\mu eV/c^2$ and 1 eV/c^2 [23].

The allowed masses of the QCD axions are too low to induce a detectable signal in DARWIN, but the detector can look for the so-called axion-like particles (ALPs) instead. These particles cannot necessarily solve the CP problem, but they are predicted by several models and could also be the dark matter in the Universe [21]. The mass of ALPs is independent of f_a and could be in the keV/c^2 range.
In addition, there are QCD axions that arise from lower symmetry breaking scales. They are not dark matter candidates but still could be produced in the Sun through Compton scattering, Bremsstrahlung or axio-recombination and axio-deexcitation in large numbers [24]. Such solar axions may not directly tell us anything about axionic dark matter, but would be evidence of physics beyond the standard model

[25].

2.3 Detection of dark matter

Despite the large abundance of dark matter in the Universe, no other than its gravitational interaction with ordinary matter has been observed yet. Current experiments try to detect other forms of interactions between dark matter and standard model particles with three different approaches illustrated in figure 4.

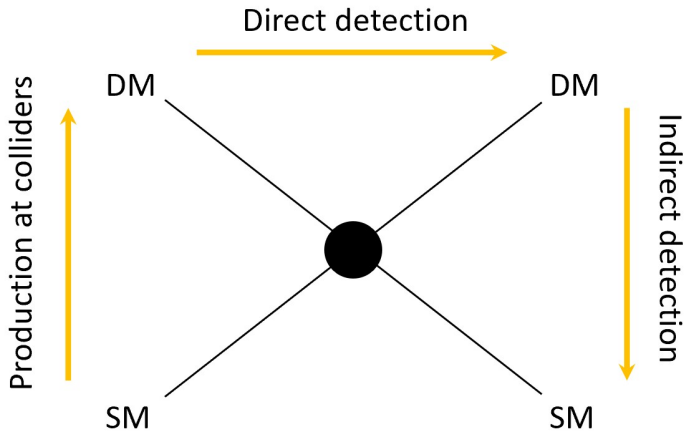

Figure 4: Detection methods for interactions between dark matter (DM) and standard model particles (SM). The arrows represent the time axis and the black dot the interaction vertex.

Production in collision experiments

Colliders were very successful to explore the standard model particles, and it is obvious to use them also for dark matter searches. High energy colliders such as the LHC try to produce dark matter particles and detect them [26]. Though, such particles cannot be measured directly, as they just pass through the detector, without any interaction. However, the production process would leave some known particles behind and because of the conservation of momentum, dark matter particles could be traced back through a missing momentum in the collision [19]. The searches of ATLAS and CMS at the LHC have not shown any evidence for such an event yet.

Indirect detection

Indirect detection experiments aim to observe standard model particles and radiation that result from an annihilation process of dark matter particles. These could

be neutrinos, gamma rays, antiprotons or positrons. The experiments perform their searches where the dark matter density is expected to be high and annihilation processes are therefore more likely, such as in the galactic center and halo or dwarf spheroidal galaxies [27]. So far, some experiments have detected unusual signals that could originate from dark matter annihilation, as for example an observed excess of positrons measured by the PAMELA experiment [28] and later by the AMS-02 [29]. However, the signals remain ambiguous as all these experiments face the challenge to differentiate a possible dark matter signal from sources of astrophysical background [19].

Direct detection

The third type of experiments tries to detect a signal from an interaction between dark and ordinary matter. For WIMPs, this is a nuclear recoil, that can be spin-dependent or spin-independent [30]. Because such events are so rare due to the low scattering cross section on nucleons from 10^{-41} to 10^{-51} cm^2, direct detection experiments require a large and dense target [30]. In addition, a low energy-threshold is necessary, as the WIMPs reach the Earth with non-relativistic velocities and therefore deposit only small energies in the nuclear recoil between 1-100 keV [31]. The released energy from the interaction can be measured from three different signals: scintillation light, charge from ionization and heat in the form of phonons. This results in different detector concepts that are currently in use. Most of them measure two types of signals for background discrimination. The current CRESST III experiment for example has a $CaWO_4$ crystal as a target and detects scintillation light and phonons [32]. It reaches a very low energy threshold and can probe light WIMPs. The EDELWEISS [33] and SuperCDMS experiment [34] use germanium detectors and measure charge and heat. Detectors that are based on a dual phase noble gas time projection chamber (TPC) like the DARWIN experiment [3], use the signal from the scintillation light and the ionization.
The use of a liquid noble gas target such as liquid argon or xenon is currently the most promising concept for the direct detection. The XMASS detector [35] and the DEAP-3600 experiment [36] measure only the scintillation light, while the experiments DarkSide-50 [37], PandaX [38], LUX [39] and XENON1T [40] have a dual phase TPC. The most stringent exclusion limit on the spin-independent WIMP-nucleon interaction cross section for masses above 6 GeV/c^2 has been set by the XENON1T experiment, excluding cross sections above $4.1\times10^{-47}cm^2$ for a mass at 30 GeV/c^2.

All the mentioned experiments are located deep underground, where they are partially shielded from cosmic rays. This feature, together with the use of appropriate materials and purification systems that minimize the radioactive contamination of the target (when possible), allows these experiments to achieve an ultra-low background rate.

2.3.1 The search for axions and axion-like particles

For the search of axions and ALPs, there are some distinctive detector concepts in use. They are based on the predicted couplings to photons, electrons, and nuclei. Most current experiments focus on the conversion of the axion to two photons in a magnetic or electric field through the Primakoff effect [41]. Figure 5 gives an overview of the constraints established by previous experiments and shows the reach of future ones. Axion haloscopes such as the ADMX detector [42] search dark matter QCD axions, using a tuneable microwave cavity, in which the conversion should be enhanced. The CAST experiment at CERN [43] is a so-called helioscope that looks for solar axions that could be converted into X-rays in a magnetic field. It will be followed by a next-generation helioscope, IAXO [44]. The same idea is behind the light-shining-through-wall experiments. An example is the ALPS-II experiment, that aims to confirm that photons can convert into axions which pass then through an optic barrier and reconvert into photons afterwards [45].

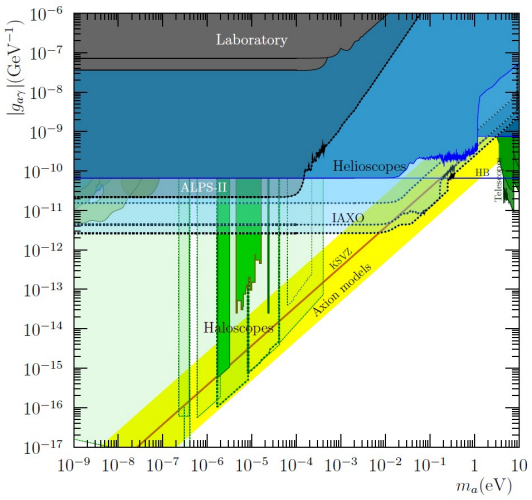

Figure 5: Summary of the exclusion regions from haloscopes and helioscopes for the coupling of photons and axions $g_{a\gamma}$ as well as the predicted reach of future experiments. Figure taken from [41].

As mentioned in section 2.2.2, liquid xenon detectors like DARWIN can also search for solar axions and galactic ALPs, by using the predicted coupling to electrons. The current XENON1T detector at the INFN Laboratori Nazionali del Gran Sasso has shown new results in June 2020, that reveal an interesting observation [25]. The recorded data shows an excess over the expected background in the energy region below 7 keV that could originate from solar axions, rejecting the null hypothesis at 3.5 σ significance. Though, the excess could also be explained by β-decays of tritium at 3.2 σ, that could be present in trace amounts in the target. A third hypothesis suggests, also at 3.2 σ, that the excess could be due to neutrinos, that have an enhanced magnetic moment. Therefore, subsequent experiments such as PandaX-4T [46], LZ [47], XENONnT [48] or DARWIN [3] are required to provide more clarity.

2.4 DARWIN: the ultimate dark matter detector

The DARWIN detector will be a future direct detection dark matter experiment using a liquid xenon target in a dual phase TPC. With a total of 50 t of liquid xenon, an ultra-low background level and a low energy threshold, it will be sensitive to various rare interactions.

The main research goal will be the detection of WIMPs, for which the detector design is being optimized. The mass and interaction cross section for WIMPs are unknown and dependent on the model, what results in a large parameter space. DARWIN can cover the entire experimentally accessible parameter space above the neutrino induced background ($\nu - line$), as shown in figure 6. This means that DARWIN will probe the dark matter candidate down to a cross section of a few $10^{-49} cm^2$ at a mass around 50 GeV/c^2 [3]. Besides WIMPs, the detector will be able to look for solar axions and ALPs as it will be discussed in section 2.4.3 in more detail. It will observe also the coherent neutrino-nucleus scattering of supernova and ^8B neu-

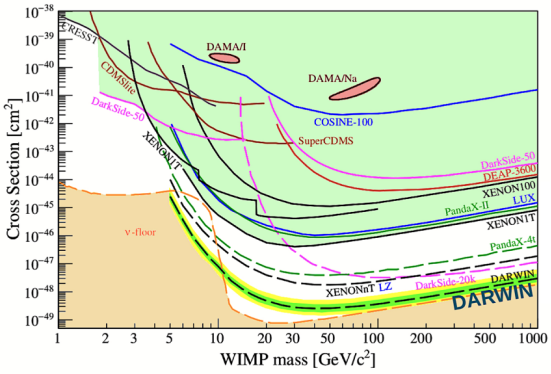

Figure 6: Sensitivity of past, current and future (dashed line) experiment to the WIMP-nucleon scattering as a function of the mass. Updated figure from [3].

trinos, detect solar neutrinos and offer the opportunity to search for the neutrinoless double beta ($0\nu\beta\beta$) decay of ^{136}Xe. The observation of this decay would confirm, that neutrinos are Majorana particle and hence their own antiparticles.
The following sections will reveal the design of the detector, its working principle and how the detector can search solar axions and ALPs.

2.4.1 Detector design

Figure 7a shows a sketch of the planned detector design. The dual phase TPC will be placed in a double-wall cryostat, which will be installed with a support structure inside a large water tank. The water will shield the detector from external radioactivity, and will be used to detect cosmic muons entering the detector. The cryostat itself will be made of titanium, that produces a lower radiogenic background than one made of a stainless steel [49]. The TPC and the cryostat will be connected to a complex cooling and purification system, that will be located outside the water tank. The first system keeps the xenon liquefied at a constant temperature around -95°. The latter is required to purify the target from electronegative impurities, to maximise the light and charge yields, as well as from radioactive contaminants, to reduce the background.
The wall around the TPC illustrated in figure 7b is made of polytetrafluoroethylene (PTFE), that can reflect efficiently the vacuum ultra-violet (VUV) scintillation light. It is enclosed by 92 copper rings that are required for the homogeneity of the applied electric field.

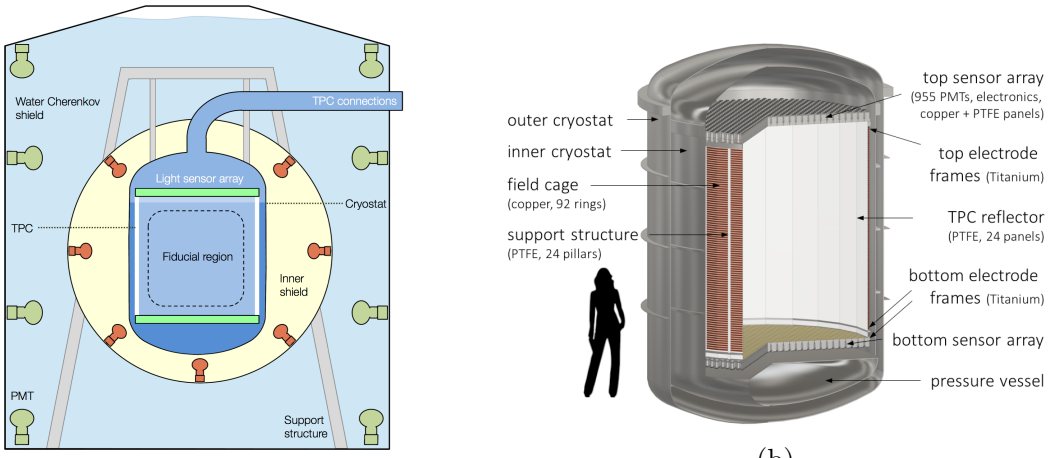

(a) (b)

Figure 7: a) Sketch of the baseline design of the entire detector structure (figure from [3]). b) The TPC, inside the double-walled titanium cryostat (figure from [49]).

2.4.2 Dual phase TPCs and signal detection

The DARWIN dual phase TPC will have a diameter and a height of 2.6 m and will contain 40 t of liquid xenon (LXe). Its design is largely based on the established concept of current detectors like XENON1T [50] and allows to precisely measure not only the deposited energy, but also the position of the interaction in the TPC. Such an interaction can be a nuclear or an electronic recoil. As illustrated in figure 8, the prompt scintillation light is released in an interaction and can be measured by photosensor arrays located at the top and bottom of the TPC. This signal is called S1. The ionization generates free electrons, that drift in an applied electric field to the top of the TPC, where the xenon is in gaseous form. There, the electrons are extracted applying a higher electric field and they generate a second delayed scintillation light. This signal is called S2. The position in the vertical z-axis can be reconstructed from the time difference between the S1 and the S2 signal. The position in the x-y plane is measured using the pattern of light in the top array. In addition, the S1/S2 ratio enables background discrimination, because an electronic recoil causes more ionization than a nuclear recoil. Hence, for the detection of WIMPs, signals from electronic recoils can be neglected, and for the solar axions and ALPs, the signal of nuclear recoils.

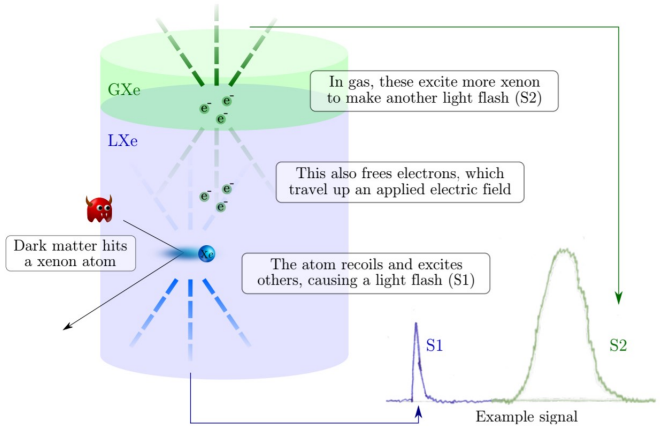

Figure 8: The signal detection in a dual phase TPC. Figure taken from [27]

The type of photosensors that measure the scintillation light at the top and the bottom of the TPC has not been decided yet. The background simulation in section 3 has implemented the photomultipliers employed in XENON1T (Hammamatsu R11410-21). But silicon photomultipliers (SiPMs) and other new types of photosensors are in consideration, that might have better properties [51, 52, 53].

2.4.3 Signal of solar axions and axion-like particles

The focus of this work is on the sensitivity of DARWIN to solar axions and ALPs. The detector will search for them by exploiting the axio-electric effect, where axions couple to electrons of the xenon target and cause atomic ionization in a similar way as in the photoelectric effect [54]. So both, solar axions and ALPs would induce electronic recoils, but their signals do not show the same characteristics. The signal from a non-relativistic ALP would be a monochromatic peak at their rest mass, because their kinetic energy is negligible and their mass is fully converted into energy. The signal of a solar axion with a certain mass is expected to cover a energy spectrum with a peak close to the axion mass and a decreasing characteristic above it [55]. The mass of solar axions is thereby small compared to their kinetic energy.

3 Simulation of the electronic recoil background

The identification of a signal always requires a precise understanding of the background spectrum. This allows to differentiate between background events and signals that could originate from an unknown particle.
The background sources of DARWIN can be divided into two groups: The intrinsic background from radionuclides in the target and from cosmic particles directly interacting with the xenon atoms. And the external background, that is induced by radioactive decays in the detector materials surrounding the target. As solar axions and ALPs would recoil off an electron, the background of nuclear recoils can be neglected for this work.
In the following, the electronic recoil background model for the DARWIN detector is completed. This work uses the results of a previous background study, that the DARWIN collaboration has performed for the $0\nu\beta\beta$ decay of ^{136}Xe [49], and adds the two missing isotopes ^{40}K and ^{85}Kr. These isotopes contribute to the low-energy background that is not relevant for the $0\nu\beta\beta$ decay of ^{136}Xe but coincides with the region of interest for the search of solar axions and ALPs.

3.1 Sources of background

Despite the selection of very radio-pure materials, the isotope ^{40}K is contained in most detector materials and contributes to the external background. It decays via beta decay (89.25%) and to a lesser extent via electron capture and a subsequent gamma decay (10.55%), as shown in figure 9a.

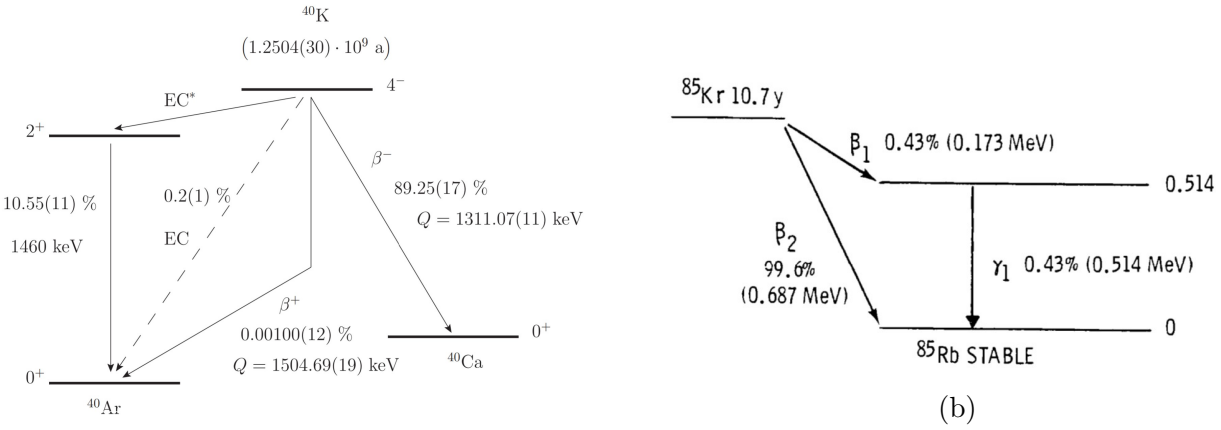

(a) (b)

Figure 9: The decay schemes of ^{40}K (from [56]) and ^{85}Kr (from [57]).

^{85}Kr contributes to the intrinsic background and is homogeneously distributed in the xenon target. Commercially available xenon is obtained through the distillation of liquid air and is therefore always contaminated with natural krypton. As illustrated in figure 9b, the isotope ^{85}Kr decays to ^{85}Rb, either directly via beta decay (99.6%), or very rarely via beta decay and a subsequent gamma ray emission (0.43%). Both channels produce an electronic recoil signal. To reduce the contribution of this background source, DARWIN's purification system will remove krypton to some extent by cryogenic distillation. The concentration of krypton that DARWIN is expected to reach is discussed in the next section.

3.2 Data generation

To obtain the background contribution of ^{40}K and ^{85}Kr, their radioactive decays and the subsequent interactions in the target are simulated. The generation of those events is done with the GEANT4 simulation toolkit [58]. It allows to implement a realistic detector design of DARWIN and generate decay events. The particles simulated with GEANT4 are propagated through the detector until the xenon target, and the position and energy of each interaction is recorded. Table 1 shows all the simulated detector components and the amount of liquid xenon. The implementation in GEANT4 is adopted from the DARWIN collaboration.

Material	Component	Mass [kg]	Total mass [kg]
Copper	92 field shaping rings	678.302	1199.25
	2 structural support layers	520.948	
PTFE	TPC walls (3 mm thickness)	146.804	301.16
	24 structural support pillars	84.268	
	Reflector + sliding panels	70.083	
Titanium	Inner cryostat	2093.83	5507.8
	Outer cryostat	3038.22	
	Bottom pressure vessel	375.706	
PMTs (3")	1900 units of 190g	-	363.7
PMT bases	1900 units of 3g	-	5.73
Liquid xenon	-	-	49'330.5

Table 1: Simulated detector components together with their corresponding masses.

The PMTs and the PMT bases are not simulated individually but a simplified geometry is used. Two simple disks, at the top and bottom of the TPC, represent them, accounting for their proper amount of mass and the associated radioactive contamination. This allows to compare the background contribution of the PMTs to other types of photosensors by substituting simply the mass and the radiogenic activity.

3.2.1 Simulation of ^{40}K

The decay of ^{40}K is simulated in each detector material separately. In this way the contribution of each material to the background can be evaluated. The number of generated events in the different materials is indicated in table 2. It is chosen such that it is large enough to obtain the proper shape of the spectrum and ensure a statistically valid result, but, at the same time, keep the running time of the simulation reasonable.

Material	Number of generated events	Effective lifetime in years
Copper	10^7	0.7
PTFE	10^7	3.1
Titanium	10^8	1.1
PMTs	10^8	0.14
PMT bases	10^7	0.6

Table 2: Number of generated events and effective lifetime for ^{40}K.

The time that it takes for the generated events to happen in DARWIN is denoted as effective lifetime in table 2. It can be determined as follows:

$$T = \frac{N}{W \cdot M \cdot A \cdot (60 \cdot 60 \cdot 24 \cdot 365)} \tag{2}$$

where N is the number of generated events, W is the weighting factor, M is the mass (in kg) and A the specific activity (in Bq/kg) of a material. The numbers are such as to obtain the lifetime in years. This will be used in section 3.3 for the normalization of the background spectrum. The values for the activity of the materials, indicated in table 3, are taken as fixed values and were measured for the XENON1T experiment [59] and the LZ experiment [60]. For PTFE and titanium, the value corresponding to the upper limit is used conservatively for the simulation.

It is assumed that the materials used for DARWIN will have a similar or smaller activity. The weighting factor W is required because GEANT4 (version 10) does not generate N whole decay chains of the starting isotope but counts every single decay in the decay chain as an event. For ^{40}K, the weighting factor is 1.0 ± 0.0 as previous simulation studies for DARWIN have calculated.

Material	Reference	Activity [mBq/kg]
Copper	[59]	0.4
PTFE	[59]	<0.343
Titanium	[60]	<0.54
PMTs	[59]	62.7
PMT bases	[59]	93.2

Table 3: Activity of ^{40}K in each material.

3.2.2 Simulation of ^{85}Kr

In a similar manner, the decay process of ^{85}Kr is simulated in the total amount of liquid xenon. The effective lifetime indicated in table 4 is again calculated with eq. 2. The weighting factor W is 1.0045 ± 0.0002 and has also been calculated by previous simulations for DARWIN.

Material	Number of generated events	Effective lifetime in years
LXe	10^7	0.7

Table 4: Number of generated events and effective lifetime for ^{85}Kr

In this case, the activity depends on the removal of natural krypton from xenon. The current XENON1T experiment reaches a concentration of about 26 ppq[1] by cryogenic distillation [61]. It is assumed for this simulation that DARWIN can reduce the concentration that has been achieved in XENON1T by a factor of about 10, to 2 ppq. The activity is then given by:

$$A = \frac{N_A \cdot C_{nat} \cdot C_{85} \cdot ln(2)}{t_{1/2} \cdot M_{mol}} \tag{3}$$

[1] ppq: parts per quadrillion

with the molar mass M_{mol}, the Avogadro constant N_A and the concentrations C_{nat}, C_{85} and half-life $t_{1/2}$ given in table 5.

Material	Reference	^{nat}Kr / Xe (C_{nat})	^{85}Kr / ^{nat}Kr (C_{85})	half-life $t_{1/2}$
LXe	[61]	2 ppq	$2 \cdot 10^{-11}$	10.76 years

Table 5: Concentrations and half-life of ^{85}Kr

3.3 Data processing and Cuts

The energy depositions and positions of the generated events are processed in further steps to apply the event selection (including fiducialisation) into the simulation and to consider the limited energy and spatial detector resolution.
In a first step, the generated data is processed by a density based spatial clustering algorithm. It is called MCProcessor and was developed by the DARWIN collaboration. The algorithm, depending on the z-position of the interaction, groups the energy depositions that occur within a radius of 15 mm (on average) and returns the weighted position and the combined energy deposition of the resulting cluster. This enables DARWIN to classify the interaction as single and multi-site events. Single-site events contain only one cluster, whereas multi-site events contain several clusters. The correct distinction between them allows to select only single-site events for this background model. Axions and ALPs would interact with the target through the axio-electric effect [54], which is a single scatter event. Hence, the multi site signals can be neglected for this search. This reduces the background that has to be considered for axions and ALPs substantially and thus improves the sensitivity.
To take the energy resolution of the detector into account, the energy of each cluster is smeared according to a Gaussian distribution. The standard deviation is given by:

$$\frac{\sigma_E}{E} = \frac{a}{\sqrt{E}} + b \tag{4}$$

with the parameters determined by the XENON1T experiment [62]: $a = 0.3171 \pm 0.0065$ [keV$^{\frac{1}{2}}$] and $b = 0.0015 \pm 0.0002$. Analogously, the position of the clusters is smeared with $\sigma_{x,y,z} = 10$ mm to account for the finite position resolution of the detector.

3.3.1 Fiducial volume cut

In the case of ^{40}K, another significant reduction of the background rate can be achieved by a fiducial volume cut. Due to the good shielding capability of the liquid xenon, most of the external background events are close to the walls of the TPC (see figure 10).

Thus, the background rate is reduced by considering only the signals from a smaller target volume. Of course, the target mass cannot be chosen arbitrarily small, since a smaller target would imply a diminished interaction probability. For this study, a volume of 30 t is selected. The shape of the volume is an optimized super-ellipsoide (with minimum background for the given mass) that is defined by eq. 5. The parameters indicated in table 6 are adopted from a sensitivity study for solar neutrinos performed by the DARWIN collaboration [63].

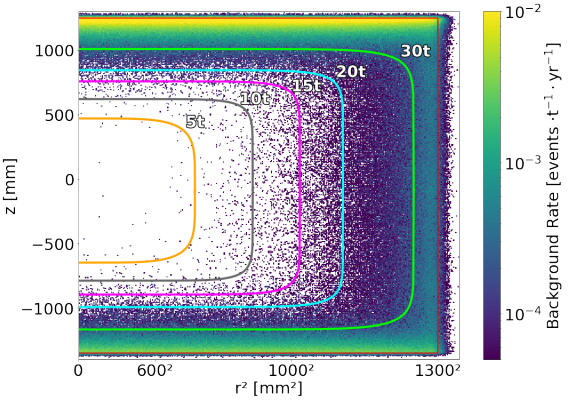

Figure 10: Distribution of the external background inside the TPC of DARWIN. Figure from the background study for the $0\nu\beta\beta$ decay [49].

$$\left(\frac{Z(mm)+z_0}{Z_{max}}\right)^t + \left(\frac{X(mm)^2+Y(mm)^2}{R_{max}^2}\right)^{\frac{t}{2}} < 1 \tag{5}$$

Fiducial Mass [t]	R_{max} [mm]	Z_{max} [mm]	z_0 [mm]	t
30	1220	1234.5	55	5

Table 6: Paramter for an optimzed super-ellipsoide with 30 t of fiducial mass

As ^{85}Kr is an intrinsic background source that is homogeneously distributed in the target, a fiducial volume cut cannot reduce the background rate and is therefore not applied.

To conclude the data processing, the resulting background spectra are normalized to the expected background rate of DARWIN in (events/t/year/keV)) by using the effective lifetime indicated in section 3.2.

3.4 Results

In the following section, the resulting background spectra for the two simulated isotopes are shown. The total background spectrum summarizing all sources is presented and discussed as well. The focus of this study is on the energy region below 500 keV as it is the region of interest for the search of solar axions and ALPs. Nevertheless, the whole energy region is shown as the obtained background model can be used for other science channels that DARWIN will study.

3.4.1 ^{40}K Spectrum

To ensure that the detector geometry and the decay process is implemented correctly in GEANT4, the primary positions of the ^{40}K isotopes are plotted in the different materials as shown in figure 11.

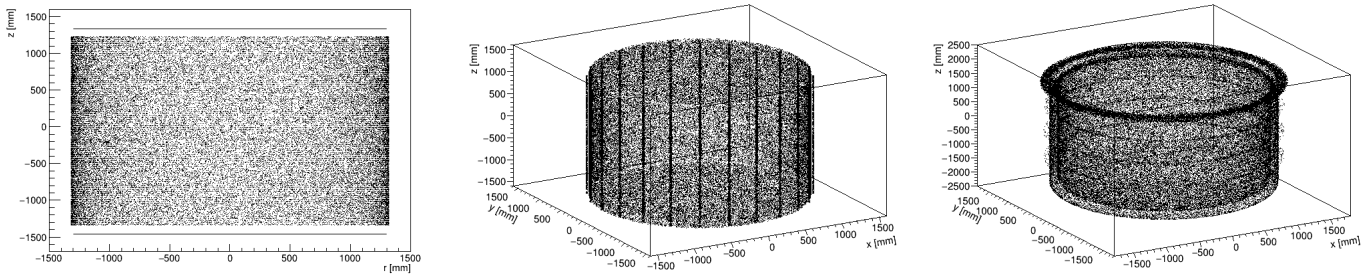

(a) Copper (b) PTFE (c) Cryostat

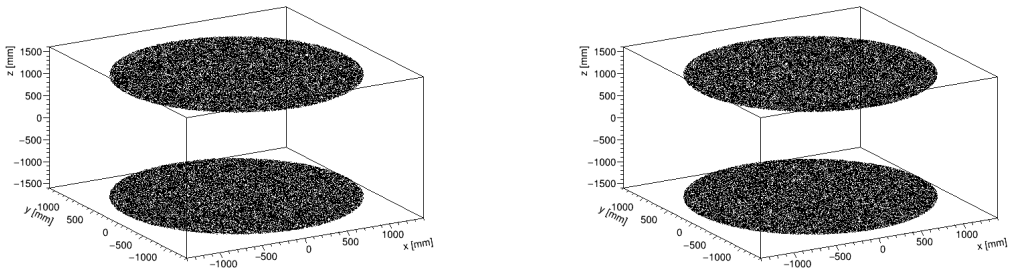

(d) PMTs (e) PMT bases

Figure 11: Primary positions of the generated events of ^{40}K decays.

Figure 12 shows the background spectrum of ^{40}K and the contribution of the different materials. The spectrum is a superposition of the beta and gamma decays of the isotope. However, the contribution of the gamma decay is dominating, represented by the peak at 1460 keV. The gamma decay is far less likely than the beta decay,

but the gamma radiation can pass easily through the detector and deposit the whole energy, whereas most electrons from the beta decay lose their energy on their way to the fiducial target mass.

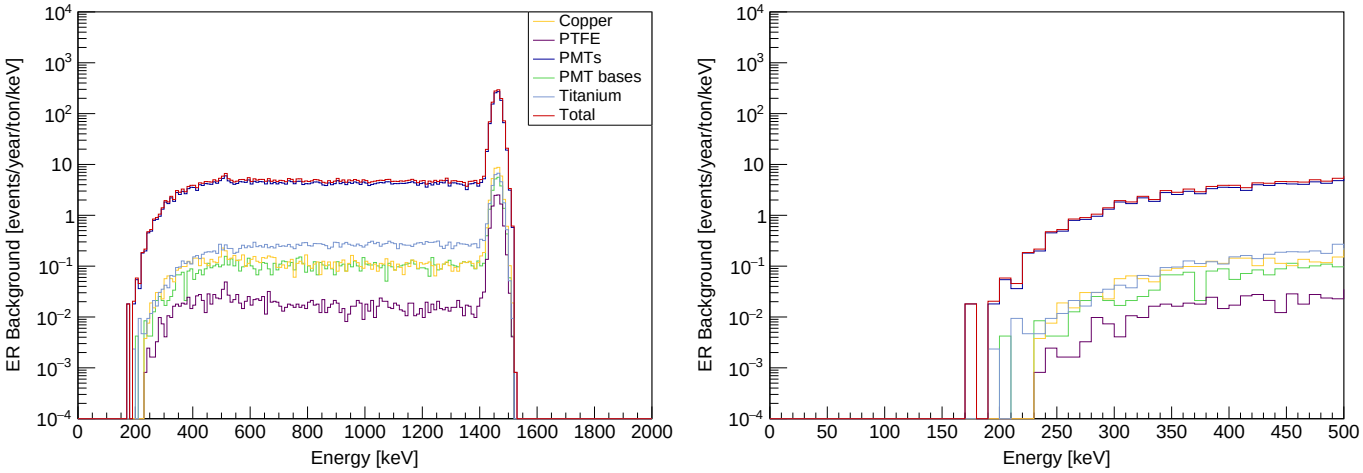

(a) (b)

Figure 12: Total background spectrum of ^{40}K and the different components in the whole energy region (a) and below 500 keV (b).

In the whole energy region, the contribution of the PMTs far outweighs the contributions of the other materials, what is due to the high specific activity. This shows the relevance of evaluating other types of photosensors with a lower level of radioactivity like SiPMs.

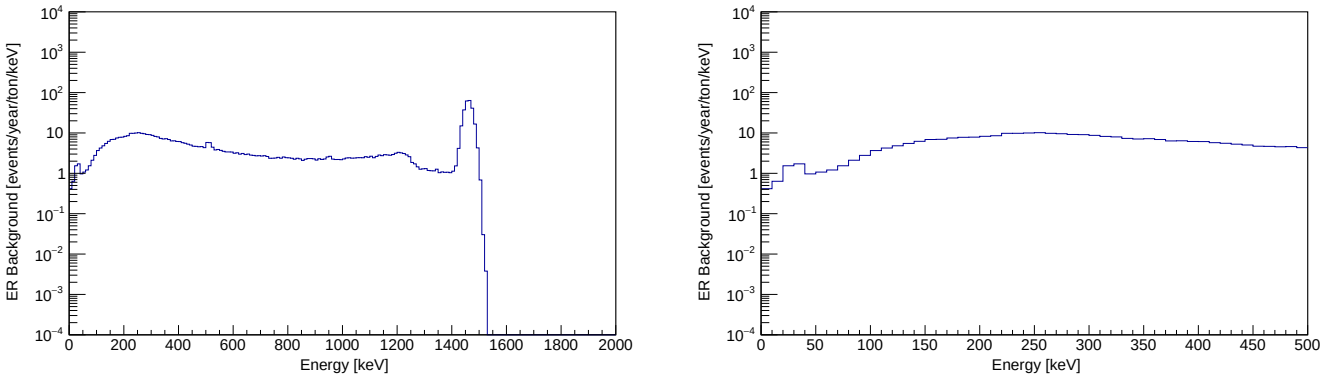

(a) (b)

Figure 13: The background spectrum from the radioactive decays of ^{40}K in copper before the fiducial volume cut.

Figure 13 shows as an example the background spectrum of copper before the fiducial volume cut. The comparison with figure 12 demonstrates the successful background reduction by the cut. It is particularly efficient in the region below 200 keV because most low-energy radiation and particles interact already in the outer region of the target and cannot reach the fiducial mass. In fact, the spectrum shows no background events after the fiducial volume cut below 200 keV. Though, it is to mention that some events are expected in this region during the lifetime of DARWIN, but the number of simulated events is not large enough to show this. In general, the main source of uncertainty for this simulation is due to the number of simulated events.

3.4.2 ^{85}Kr Spectrum

The primary positions of the ^{85}Kr isotope in figure 14a show the homogeneous distribution in xenon. The background spectrum of the isotope, see figure 14b, shows the typical behaviour of a beta decay. The gamma decay is so rare that it contributes only with a tiny peak at 514 keV to the spectrum.

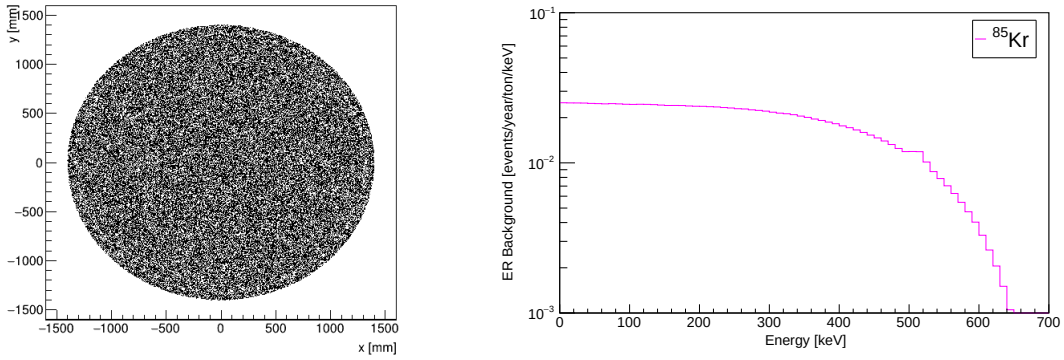

(a) (b)

Figure 14: a) Primary positions (in the x-y plane) of ^{85}Kr in the xenon target. b) Background spectrum of ^{85}Kr.

3.4.3 Total background

To complete the electronic recoil background model of DARWIN, the isotopes ^{40}K and ^{85}Kr are added to the background spectrum that has been produced for the sensitivity study of the $0\nu\beta\beta$ decay [49]. The different sources of the external background are shown together, this includes ^{238}U, ^{232}Th, ^{235}U, ^{60}Co, ^{137}Cs and ^{44}Ti. Figure 15 reveals the contribution of ^{40}K to the total external background. The

peak originating from ^{40}K is not in the region of interest for axions and ALPs. Nevertheless, the contribution of the isotope to the region below 500 keV accounts for about 10% of the external background and is therefore significant.

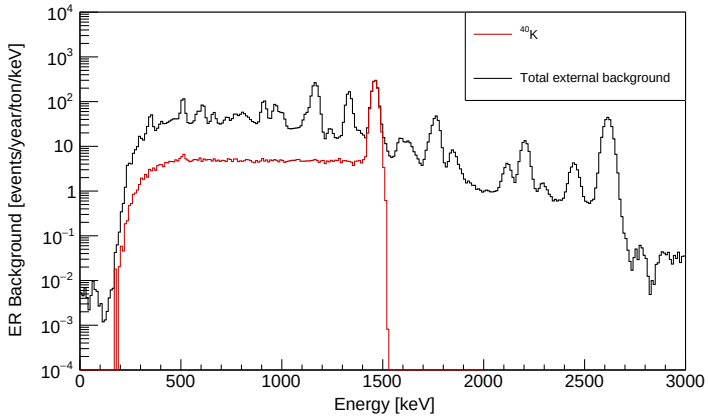

Figure 15: Contribution of ^{40}K to the total material induced background for a fiducial mass of 30 t.

The total background for the search of solar axions and ALPs is presented in figure 16. It results from the sum of the external background and all contributions of the intrinsic background which are shown separately in the figure. Besides ^{85}Kr that is simulated by this work, the following other sources contribute to the intrinsic background (simulated by [49]):

- ^{222}Rn is emanated by detector components and can reach the xenon, where it distributes itself homogeneously. It has been simulated assuming an activity of 0.1 $\mu Bq/kg$.
- The $2\nu\beta\beta$ decay of ^{136}Xe: natural xenon contains 8.9% of ^{136}Xe and the decay of the isotope has the half-life of 2.2×10^{21} years.
- ^{137}Xe is produced by the in situ cosmogenic activation of the ^{136}Xe isotope and has been simulated assuming a production rate of 6.9 atoms/(t·yr).
- The neutrino-electron scattering interactions of solar neutrinos: All components of the solar flux are considered. Below 500 keV the dominant contribution comes from pp-neutrinos and ^{7}Be-neutrinos.

Up to 100 keV, solar neutrino interactions and the $2\nu\beta\beta$ decay of ^{136}Xe are dominating the background spectrum. The solar neutrinos are an irreducible background

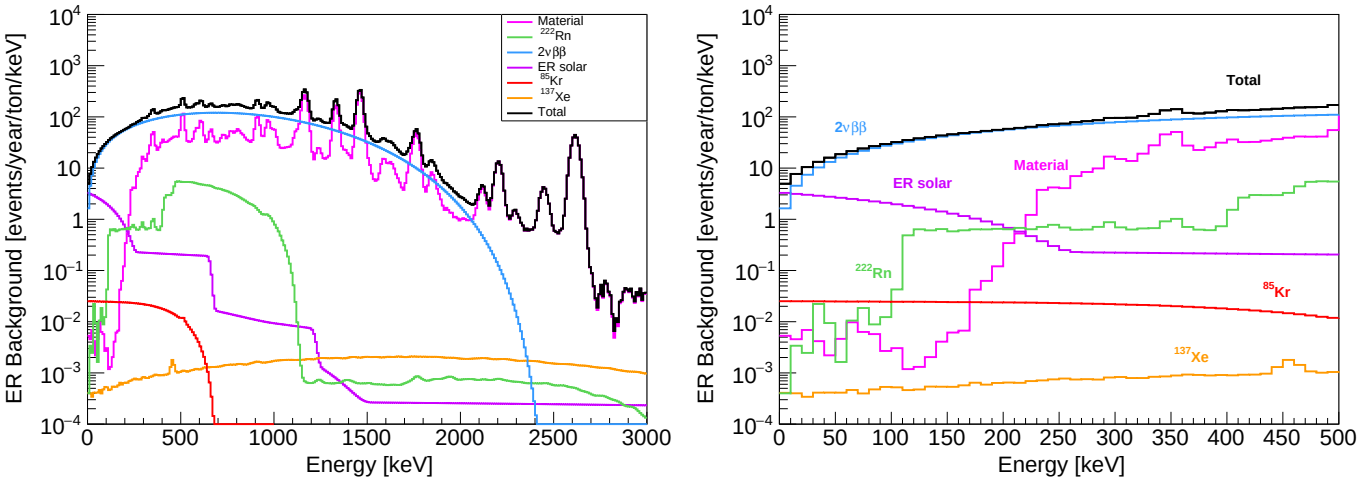

(a) (b)

Figure 16: All the components of the total background spectrum for the fiducial volume of 30 t in the whole energy region (a) and below 500 keV (b).

source, but the isotope ^{136}Xe could be removed from the target. Thus, it is shown in section 5, how the removal of this isotope would influence the sensitivity of DARWIN. In the energy region between 100 and 500 keV, the material induced background becomes relevant together with the $2\nu\beta\beta$ decay.

The simulated ^{85}Kr contributes to the low-energy background but its contribution is small because of the efficient removal of krypton from the target. In conclusion, the two isotopes ^{85}Kr and ^{40}K simulated by this work are not the main background sources in the region of interest for solar axions and ALPs. However, a proper background model has to be simulated completely. With ^{85}Kr and ^{40}K the background model of the electronic recoil channel is complete and will be used for future sensitivity studies for DARWIN, as for example the neutrinoless double electron capture of ^{124}Xe.

4 Calculation of the sensitivity

The sensitivity of DARWIN to solar axions and ALPs can be calculated by using the background model obtained in section 3. The sensitivity is defined here as the exclusion limit on the coupling strength g_{Ae} of the axio-electric effect that DARWIN could establish at a 90% confidence level (C.L.) by confirming the null hypothesis. Thus, the determined limit provides the minimum value for the coupling strength that DARWIN could probe.

4.1 Axion-like particles

The sensitivity for the ALPs is calculated with an analytical approach, following [55]. All quantities used in this section are summarized in table 7.

Symbol	Quantity	Unit
m_A	Axion mass	$[keV/c^2]$
g_{Ae}	Axio-electric coupling constant	-
σ_A	Axio-electric cross section	[barn/atom]
σ_{pe}	Photoelectric cross section	[barn/atom]
σ_E	Standard deviation defined in eq. 4	$[keV]$
$N_{\pm 2\sigma}$	Number of background events in $m_A \pm 2\sigma_E$ range	[events]
dN/dE	Differential background rate	[events/day/kg/keV]
T	Time of data-taking	[days]
W	Fiducial mass	[kg]
r_{sn}	Signal to noise ration	-
S	90% C.L. upper limit of signal events	[events]

Table 7: Summary of the quantities used in this section.

It is assumed that the ALPs account for the whole galactic dark matter density $\rho_{DM} \sim 0.3\ GeV/cm^3$ such that the flux of ALPs reaching earth Φ is given by eq. 6 [55]:

$$\Phi[/cm^2/s] = \frac{\rho_{DM} v_A}{m_A} = \frac{9 \times 10^{15}}{m_A} \times \beta_A \tag{6}$$

with the mean axion velocity divided by the speed of light $\beta_A \sim 10^{-3}$.
In addition, the cross section of the axio-electric effect σ_A is proportional to the

photoelectric cross section σ_{pe} (see figure 17) in the following way [54]:

$$\sigma_A(E) = \sigma_{pe}(E)\ \frac{g_{Ae}^2}{\beta_A}\ \frac{3E^2}{16\pi\alpha m_e^2}\ \left(1 - \frac{\beta_A^{2/3}}{3}\right) \tag{7}$$

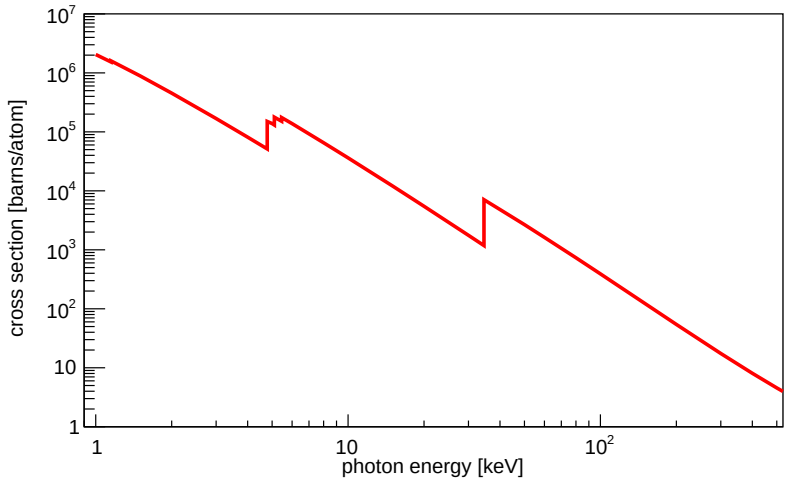

Figure 17: Photoelectric cross section for the xenon atom between 1-500 keV. Data from the NIST Photon Cross Sections Database [64].

Using the equations, the interaction rate of ALPs with the xenon target can be expressed by eq. 8 [55].

$$R[/kg/day] = \frac{1.29 \times 10^{19}}{A}\ {g_{Ae}}^2\ m_A[keV/c^2]\ \sigma_{pe}[barns] \tag{8}$$

The total number of singal events is then given by $R \times W \times T$.

To determine the sensitivity on the coupling constant g_{Ae}, the null hypothesis is considered. It corresponds to the case where DARWIN will observe only the expected background. The upper confidence limit on the number of signal events for the background only case at a 90% C.L. is given by [55]:

$$S = r_{sn}\sqrt{N_{\pm 2\sigma}} \tag{9}$$

where $N_{\pm 2\sigma}$ is the number of background events in a $\pm 2\sigma_E$ energy window around the deposited energy and $r_{sn} = 1.7$ is the signal to noise ratio that corresponds to a 90% C.L. for $N_{\pm 2\sigma} > 50$ [55]. Given the quantities in table 7, N can be calculated

as follows:

$$N_{\pm 2\sigma} = 4\sigma_E \times \frac{dN}{dE} \times TW \tag{10}$$

The upper limit of signal events S is set equal to $R \times W \times T$ with the rate R defined in eq. 8. S is expressed using the stated value for r_{sn} and definition of N from eq. 10. By rearranging the equation, the sensitivity is obtained in terms of the coupling constant g_{Ae} of the axio-electric effect:

$$g_{Ae}(90\% C.L.) = \frac{4.5 \times 10^{-9}}{m_A{}^{\frac{1}{2}}} \left(\frac{r_{sn}}{\sigma_{pe}}\right)^{\frac{1}{2}} \left(\frac{\sigma_E \times (dN/dE)}{W \times T}\right)^{\frac{1}{4}} \tag{11}$$

Eq. 11 shows that the sensitivity depends on the fourth root of the experimental parameters.

Results

Considering 10 years of data-taking, 30 t fiducial mass, the total background from section 3 and the energy resolution of XENON1T, the coupling limit is obtained as a function of the mass as shown in figure 18. The calculation implies that DARWIN can reach a minimum value for g_{Ae} of 1.8×10^{-15} at a mass of 1 keV/c^2. This mass corresponds to the energy-threshold of the detector. The lower sensitivity at higher masses is due to the strongly decreasing cross section. The background and σ_E that increase for higher energy depositions have only a very small influence in comparison. Furthermore, the same features of the cross section are observed in the sensitivity.

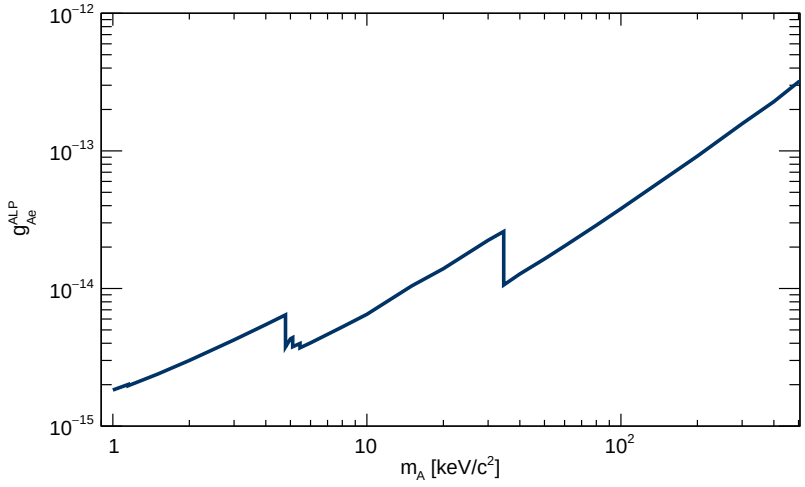

Figure 18: Sensitivity of DARWIN to ALPs as a function of their mass.

4.2 Solar axions

For the solar axions, the sensitivity to the coupling constant g_{Ae} is obtained by a scaling approach as there is no analytical equivalent to eq. 11.
The flux of solar axions reaching earth can be calculated from the production processes in the sun. As mentioned in section 2.2.2, the axions are produced in different processes but we consider only the dominant processes arising from Compton scattering and Bremsstrahlung. The signal event rate in the xenon target is then given by the convolution of the solar axion flux and the axio-electric cross section, requiring a numerical integration for its evaluation. This obstacle can be circumvented as the signal event rate is the same for all experiments with a xenon target. Thus, the limit on the coupling g_{Ae} can be determined by scaling the result from a previous experiment to DARWIN, considering only the experimental parameters that differ: the background rate, the energy resolution, the fiducial mass and the time of data-taking. As the flux and the cross section are proportional to ${g_{Ae}}^2$, the limit depends on the eight root of the experimental parameters [55].

$$g_{Ae} \sim \left(\frac{dN/dE}{W \times T}\right)^{\frac{1}{8}} \tag{12}$$

The coupling constant is scaled from the latest results from the XENON1T experiment. As mentioned in section 2.3.1, the experiment observed an excess of events at the low energies such that it is able to exclude values of g_{Ae} above 3.7×10^{-12} in the range of electronic recoil energies between 1-30 keV [25].
Table 8 shows a comparison of the experimental parameters. The background rate corresponds to the average rate in the selected energy region (1-30 keV). As it is assumed that DARWIN will have the same energy resolution as XENON1T, it is not considered and does not appear in eq. 12 for that reason.

Experiment	Background rate [events/year/t/keV]	W [t]	T [years]
XENON1T [25]	76	1.042	0.62
DARWIN	7.7	30	10

Table 8: Comparison between the experimental parameters of XENON1T and DARWIN for the energy range of 1-30 keV.

Results

The lower background and larger exposure of DARWIN improves the limit compared to XENON1T by a factor of around 3, such that DARWIN will be able to exclude values of g_{Ae} above 1.3×10^{-12}. The energy range (1-30 keV) is not identical to the mass range as the solar axions do not produce a monochromatic peak at their rest mass like the ALPs but deposit their kinetic energy.

5 Discussion

The DARWIN experiment will be able exclude values of the axio-electric coupling strength g_{Ae} above 1.3×10^{-12} for solar axions in the mass range of $10^{-5} < m_A < 1\ keV/c^2$ and values of g_{Ae} above 1.8×10^{-15} for ALPs at the mass of $1\ keV/c^2$. Thus, the obtained result confirms that DARWIN will reach an unprecedented sensitivity for the direct detection of solar axions (being a LXe TPC) and ALPs and in the case of no signal detected it will set a new exclusion limit on the coupling with an exposure of 300 $t \times years$. Figure 19a shows the limits for the ALPs established by past and current experiments. DARWIN will improve the sensitivity of current experiments such as PandaX-II and XENON1T by about an order of magnitude. The exclusion limit from the XENON1T experiment is based on results from 0.65 $t \times years$ of exposure and the limit provided by PandaX-II from 0.07 $t \times years$. Both experiments are using dual phase TPCs with xenon like DARWIN.

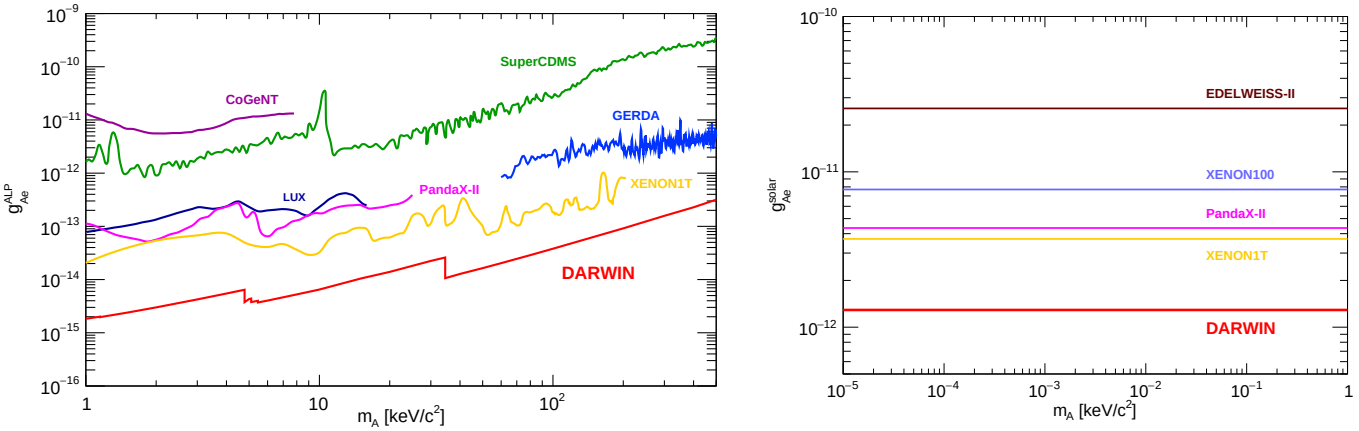

(a) (b)

Figure 19: Sensitivity of DARWIN to ALPs (a) and solar axions (b) compared to the limits obtained by current and past experiments such as CoGeNT [65], SuperCDMS [66], LUX [67], PandaX-II [68], EDELWEISS-II [69], GERDA [70], XENON100 [71] and XENON1T [25].

In the case of the solar axions, the improvement of DARWIN compared to current experiments is more modest due to the weak dependence on the experimental parameters as shown in figure 19b. Nevertheless, DARWIN would provide an excellent opportunity for the direct detection and characterisation of solar axions, which are receiving some attention because of the observed excess in XENON1T [25].

The accuracy of the presented sensitivity calculation for DARWIN depends on the successful simulation of the electronic recoil background spectrum. As some aspects of the design are not known yet, the background model completed by this work cannot reproduce the exact conditions in the future detector, but it is based on realistic and sometimes conservative assumptions. The simulation of the isotope ^{40}K for example uses for the materials the activity levels demonstrated by a current experiment and it is likely that DARWIN can implement materials with a higher radio-purity.

Removing ^{136}Xe from the target

The results of the total background spectrum in section 3.4.3 show that the dominating electronic recoil background in the region between 1-500 keV originates from the double beta decay of ^{136}Xe. Natural xenon contains 8.9% of ^{136}Xe but it could be removed from the target. Hence, it is worth examining what influence the removal of the isotope has on the sensitivity to solar axions and ALPs.
The simulated background spectrum allows to do this in a quantitative way. Because ^{137}Xe is produced by the cosmogenic activation of ^{136}Xe, not only ^{136}Xe is removed from the background spectrum but also the contribution of ^{137}Xe.

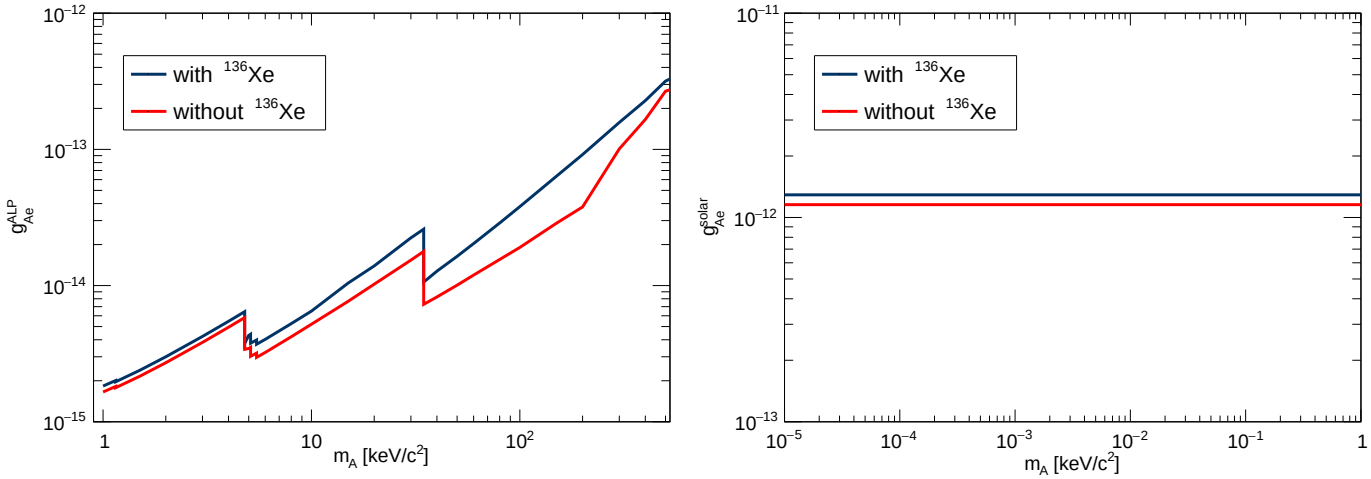

(a) (b)

Figure 20: Comparison of the sensitivity for the baseline scenario and the case where ^{136}Xe is removed.

Figure 20 shows a comparison between the baseline scenario and the case where ^{136}Xe

and ^{137}Xe are removed from the target. At 200 keV, this reduces the background by a factor of about 40. This large reduction in the background rate improves the exclusion limit of g_{Ae} for ALPs at most 2.5 times. For solar axions the improvement is more modest because of the weak dependence on the experimental parameters and the smaller reduction of the background rate in the region of interest between 1-30 keV. In this region, the solar neutrino interactions are dominant next to ^{136}Xe and are responsible for up to 50% of the total background.
Thus, by removing ^{136}Xe the sensitivity could be slightly improved for the ALPs. On the downside, the improvement on the sensitivity to solar axions is low and the removal would make it impossible to search for the $0\nu\beta\beta$ decay of ^{136}Xe with DARWIN [49].

Conclusion

The presented work completes the background spectrum of the electronic recoil channel for the DARWIN experiment by adding the isotopes ^{40}K and ^{85}Kr and calculates its sensitivity to solar axions and ALPs. This allows to compare the sensitivity of the planned detector to other experiments and to evaluate the influence of the different background sources on the sensitivity. Furthermore, the background model can be used for future sensitivity studies for DARWIN, as for example for the neutrinoless double electron capture of ^{124}Xe.
Altogether, DARWIN will provide an excellent opportunity with its ultra-low background to search not only for WIMPs but also for solar axions and ALPs and might bring some light into the puzzle of dark matter or expand our knowledge of physics beyond the standard model.

Bibliography

[1] P.A. Zyla et al. "The Review of Particle Physics. 27. Dark Matter". To be published in Prog. Theor. Exp. Phys. 2020, 083C01 (2020).

[2] Laura Baudis. "The Search for Dark Matter". In: *European Review* 26.1 (2018), pp. 70–81. DOI: 10.1017/S1062798717000783.

[3] J. Aalbers et al. "DARWIN: towards the ultimate dark matter detector". In: *JCAP* 11 (2016), p. 017. DOI: 10.1088/1475-7516/2016/11/017. arXiv: 1606.07001 [astro-ph.IM].

[4] F. Zwicky. "Die Rotverschiebung von extragalaktischen Nebeln". In: *Helvetica Physica Acta* 6 (Jan. 1933), pp. 110–127.

[5] Wolfang Kapferer. *Das Rätsel Dunkle Materie*. Berlin: Springer-Verlag, 2018, pp. 50–62.

[6] V.C. Rubin, N. Thonnard, and Jr. Ford W.K. "Rotational properties of 21 SC galaxies with a large range of luminosities and radii, from NGC 4605 /R = 4kpc/ to UGC 2885 /R = 122 kpc/". In: *Astrophys. J.* 238 (1980), p. 471. DOI: 10.1086/158003.

[7] Vera C. Rubin and Jr. Ford W.Kent. "Rotation of the Andromeda Nebula from a Spectroscopic Survey of Emission Regions". In: *Astrophys. J.* 159 (1970), pp. 379–403. DOI: 10.1086/150317.

[8] Daniel Mayani. "Photomultiplier Tubes for the XENON1T Dark Matter Experiment and Studies on the XENON100 Electromagnetic Background". PhD thesis. University of Zurich, 2016. URL: https://doi.org/10.5167/uzh-130030.

[9] J.I. Read. "The Local Dark Matter Density". In: *J. Phys. G* 41 (2014), p. 063101. DOI: 10.1088/0954-3899/41/6/063101. arXiv: 1404.1938 [astro-ph.GA].

[10] Douglas Clowe et al. "A direct empirical proof of the existence of dark matter". In: *Astrophys. J. Lett.* 648 (2006), pp. L109–L113. DOI: 10.1086/508162. arXiv: astro-ph/0608407.

[11] Chandra X-Ray Observatory. *galaxy cluster 1E 0657-56*. 2006. URL: https://chandra.harvard.edu/photo/2006/1e0657/index.html.

[12] Benoit Famaey and Stacy McGaugh. "Modified Newtonian Dynamics (MOND): Observational Phenomenology and Relativistic Extensions". In: *Living Rev. Rel.* 15 (2012), p. 10. DOI: 10.12942/lrr-2012-10. arXiv: 1112.3960 [astro-ph.CO].

[13] Scott Dodelson. "The Real Problem with MOND". In: *Int. J. Mod. Phys. D* 20 (2011), pp. 2749–2753. DOI: 10.1142/S0218271811020561. arXiv: 1112.1320 [astro-ph.CO].

[14] Wolfang Kapferer. *Das Rätsel Dunkle Materie*. Berlin: Springer-Verlag, 2018, pp. 68–76.

[15] R. Adam et al. "Planck 2015 results. I. Overview of products and scientific results". In: *Astron. Astrophys.* 594 (2016), A1. DOI: 10.1051/0004-6361/201527101. arXiv: 1502.01582 [astro-ph.CO].

[16] N. Aghanim et al. "Planck 2018 results. VI. Cosmological parameters". In: (July 2018). arXiv: 1807.06209 [astro-ph.CO].

[17] Joel R. Primack. "Cosmological Structure Formation". In: *Philosophy of Cosmology UK/US Conference*. May 2015, pp. 136–160. DOI: 10.1017/9781316535783.008. arXiv: 1505.02821 [astro-ph.GA].

[18] Stephen P. Martin. "A Supersymmetry primer". In: *Perspectives on supersymmetry. Vol.2*. Ed. by Gordon L. Kane. Vol. 21. 2010, pp. 1–153. DOI: 10.1142/9789812839657_0001. arXiv: hep-ph/9709356.

[19] Sebastian Arrenberg et al. "Working Group Report: Dark Matter Complementarity". In: *Community Summer Study 2013: Snowmass on the Mississippi*. Oct. 2013. arXiv: 1310.8621 [hep-ph].

[20] R. D. Peccei and Helen R. Quinn. "CP Conservation in the Presence of Pseudoparticles". In: *Phys. Rev. Lett.* 38 (25 June 1977), pp. 1440–1443. DOI: 10.1103/PhysRevLett.38.1440. URL: https://link.aps.org/doi/10.1103/PhysRevLett.38.1440.

[21] L.F. Abbott and P. Sikivie. "A Cosmological Bound on the Invisible Axion". In: *Phys. Lett. B* 120 (1983). Ed. by M.A. Srednicki, pp. 133–136. DOI: 10.1016/0370-2693(83)90638-X.

[22] Michael Dine, Willy Fischler, and Mark Srednicki. "A Simple Solution to the Strong CP Problem with a Harmless Axion". In: *Phys. Lett. B* 104 (1981), pp. 199–202. DOI: 10.1016/0370-2693(81)90590-6.

[23] P.A. Zyla et al. "The Review of Particle Physics. 91. Axions and other similar particles". To be published in Prog. Theor. Exp. Phys. 2020, 083C01 (2020).

[24] Javier Redondo. "Solar axion flux from the axion-electron coupling". In: *JCAP* 12 (2013), p. 008. DOI: 10.1088/1475-7516/2013/12/008. arXiv: 1310.0823 [hep-ph].

[25] E. Aprile et al. "Observation of Excess Electronic Recoil Events in XENON1T". In: (June 2020). arXiv: 2006.09721 [hep-ex].

[26] Antonio Boveia and Caterina Doglioni. "Dark Matter Searches at Colliders". In: *Ann. Rev. Nucl. Part. Sci.* 68 (2018), pp. 429–459. DOI: 10.1146/annurev-nucl-101917-021008. arXiv: 1810.12238 [hep-ex].

[27] Jelle Aalbers. "Dark matter search with XENON1T". PhD thesis. Amsterdam U., 2018, pp. 13–15.

[28] Ilias Cholis et al. "The PAMELA Positron Excess from Annihilations into a Light Boson". In: *JCAP* 12 (2009), p. 007. DOI: 10.1088/1475-7516/2009/12/007. arXiv: 0810.5344 [astro-ph].

[29] M. Aguilar et al. "First Result from the Alpha Magnetic Spectrometer on the International Space Station: Precision Measurement of the Positron Fraction in Primary Cosmic Rays of 0.5–350 GeV". In: *Phys. Rev. Lett.* 110 (2013), p. 141102. DOI: 10.1103/PhysRevLett.110.141102.

[30] Marc Schumann. "Direct Detection of WIMP Dark Matter: Concepts and Status". In: *J. Phys. G* 46.10 (2019), p. 103003. DOI: 10.1088/1361-6471/ab2ea5. arXiv: 1903.03026 [astro-ph.CO].

[31] K.A. Olive et al. "Review of Particle Physics". In: *Chin. Phys. C* 38 (2014), p. 090001. DOI: 10.1088/1674-1137/38/9/090001.

[32] A. H. Abdelhameed et al. "First results from the CRESST-III low-mass dark matter program". In: *Phys. Rev. D* 100 (10 Nov. 2019), p. 102002. DOI: 10.1103/PhysRevD.100.102002. URL: https://link.aps.org/doi/10.1103/PhysRevD.100.102002.

[33] J. Gascon. "Low-mass WIMP searches with the EDELWEISS experiment". In: *J. Phys. Conf. Ser.* 1342.1 (2020). Ed. by Ken Clark et al., p. 012064. DOI: 10.1088/1742-6596/1342/1/012064.

[34] W. Rau. "SuperCDMS SNOLAB - Status and Plans". In: *J. Phys. Conf. Ser.* 1342.1 (2020). Ed. by Ken Clark et al., p. 012077. DOI: 10.1088/1742-6596/1342/1/012077.

[35] Atsushi Takeda. "WIMP search from XMASS-I fiducial volume data with background prediction". In: *J. Phys. Conf. Ser.* 1342.1 (2020). Ed. by Ken Clark et al., p. 012080. DOI: 10.1088/1742-6596/1342/1/012080.

[36] S. Westerdale. "Analysis and Dark Matter Search Results from DEAP-3600 with 231 Live Days at SNOLAB". In: *J. Phys. Conf. Ser.* 1468.1 (2020). Ed. by Masayuki Nakahata, p. 012031. DOI: 10.1088/1742-6596/1468/1/012031.

[37] B. Bottino et al. "DarkSide: Latest results and future perspectives". In: *Nuovo Cim. C* 42.4 (2019), p. 180. DOI: 10.1393/ncc/i2019-19180-0.

[38] Qiuhong Wang et al. "Results of Dark Matter Search using the Full PandaX-II Exposure". In: (July 2020). arXiv: 2007.15469 [astro-ph.CO].

[39] Vitaly A. Kudryavtsev. "Recent Results from LUX and Prospects for Dark Matter Searches with LZ". In: *Universe* 5.3 (2019), p. 73. DOI: 10.3390/universe5030073.

[40] P. Di Gangi. "Results of the 1 tonne × year WIMP search with XENON1T". In: *Nuovo Cim. C* 42.2-3 (2019), p. 76. DOI: 10.1393/ncc/i2019-19076-y.

[41] Igor G. Irastorza and Javier Redondo. "New experimental approaches in the search for axion-like particles". In: *Prog. Part. Nucl. Phys.* 102 (2018), pp. 89–159. DOI: 10.1016/j.ppnp.2018.05.003. arXiv: 1801.08127 [hep-ph].

[42] Gray Rybka. "Direct Detection Searches for Axion Dark Matter". In: *Phys. Dark Univ.* 4 (2014). Ed. by Frank Avignone and Wick Haxton, pp. 14–16. DOI: 10.1016/j.dark.2014.05.003.

[43] Martin Karuza. "The CAST Experiment: Status Report". In: *13th Patras Workshop on Axions, WIMPs and WISPs*. 2018, pp. 39–42. DOI: 10.3204/DESY-PROC-2017-02/karuza_marin.

[44] E. Armengaud et al. "Conceptual Design of the International Axion Observatory (IAXO)". In: *JINST* 9 (2014), T05002. DOI: 10.1088/1748-0221/9/05/T05002. arXiv: 1401.3233 [physics.ins-det].

[45] Robin Bähre et al. "Any light particle search II —Technical Design Report". In: *JINST* 8 (2013), T09001. DOI: 10.1088/1748-0221/8/09/T09001. arXiv: 1302.5647 [physics.ins-det].

[46] Hongguang Zhang et al. "Dark matter direct search sensitivity of the PandaX-4T experiment". In: *Sci. China Phys. Mech. Astron.* 62.3 (2019), p. 31011. DOI: 10.1007/s11433-018-9259-0. arXiv: 1806.02229 [physics.ins-det].

[47] D.S. Akerib et al. "The LUX-ZEPLIN (LZ) Experiment". In: *Nucl. Instrum. Meth. A* 953 (2020), p. 163047. DOI: 10.1016/j.nima.2019.163047. arXiv: 1910.09124 [physics.ins-det].

[48] E. Aprile et al. "Projected WIMP Sensitivity of the XENONnT Dark Matter Experiment". In: (July 2020). arXiv: 2007.08796 [physics.ins-det].

[49] F. Agostini et al. "Sensitivity of the DARWIN observatory to the neutrinoless double beta decay of ^{136}Xe". In: (Mar. 2020). arXiv: 2003.13407 [physics.ins-det].

[50] E. Aprile et al. "The XENON1T Dark Matter Experiment". In: *Eur. Phys. J. C* 77.12 (2017), p. 881. DOI: 10.1140/epjc/s10052-017-5326-3. arXiv: 1708.07051 [astro-ph.IM].

[51] L. Baudis et al. "Performance of the Hamamatsu R11410 Photomultiplier Tube in cryogenic Xenon Environments". In: *JINST* 8 (2013), P04026. DOI: 10.1088/1748-0221/8/04/P04026. arXiv: 1303.0226 [astro-ph.IM].

[52] Laura Baudis et al. "Characterisation of Silicon Photomultipliers for Liquid Xenon Detectors". In: *JINST* 13.10 (2018), P10022. DOI: 10.1088/1748-0221/13/10/P10022. arXiv: 1808.06827 [physics.ins-det].

[53] Daniel Ferenc, Andrew Chang, and Marija Šegedin Ferenc. "The Novel ABALONE Photosensor Technology: 4-Year Long Tests of Vacuum Integrity, Internal Pumping and Afterpulsing". In: (Mar. 2017). arXiv: 1703.04546 [physics.ins-det].

[54] A.V. Derbin et al. "Constraints on the axion-electron coupling constant for solar axions appearing owing to bremsstrahlung and the Compton process". In: *JETP Lett.* 95 (2012), pp. 339–344. DOI: 10.1134/S002136401207003X. arXiv: 1206.4142 [hep-ex].

[55] K. Arisaka et al. "Expected sensitivity to galactic/solar axions and bosonic super-WIMPs based on the axio-electric effect in liquid xenon dark matter detectors". In: *Astroparticle Physics* 44 (2013), pp. 59–67. ISSN: 0927-6505. DOI: https://doi.org/10.1016/j.astropartphys.2012.12.009. URL: http://www.sciencedirect.com/science/article/pii/S0927650512002344.

[56] Josef Pradler, Balraj Singh, and Itay Yavin. "On an unverified nuclear decay and its role in the DAMA experiment". In: *Physics Letters B* 720 (Oct. 2012). DOI: 10.1016/j.physletb.2013.02.033.

[57] Pacific Northwest Laboratory, P.J. Mellinger, and United States. Department of Energy. *85Kr Management Trade-offs, a Perspective to Total Radiation Dose Commitment*. Department of Energy, Pacific Northwest Laboratory, 1980. URL: https://books.google.ch/books?id=qTFLuwEACAAJ.

[58] S. Agostinelli et al. "GEANT4–a simulation toolkit". In: *Nucl. Instrum. Meth. A* 506 (2003), pp. 250–303. DOI: 10.1016/S0168-9002(03)01368-8.

[59] E. Aprile et al. "Material radioassay and selection for the XENON1T dark matter experiment". In: *The European Physical Journal C* 77.12 (Dec. 2017). ISSN: 1434-6052. DOI: 10.1140/epjc/s10052-017-5329-0. URL: http://dx.doi.org/10.1140/epjc/s10052-017-5329-0.

[60] D.S. Akerib et al. "Identification of Radiopure Titanium for the LZ Dark Matter Experiment and Future Rare Event Searches". In: *Astropart. Phys.* 96 (2017), pp. 1–10. DOI: 10.1016/j.astropartphys.2017.09.002. arXiv: 1702.02646 [physics.ins-det].

[61] E. Aprile et al. "Removing krypton from xenon by cryogenic distillation to the ppq level". In: *Eur. Phys. J. C* 77.5 (2017), p. 275. DOI: 10.1140/epjc/s10052-017-4757-1. arXiv: 1612.04284 [physics.ins-det].

[62] E. Aprile et al. "Energy resolution and linearity in the keV to MeV range measured in XENON1T". In: (Mar. 2020). arXiv: 2003.03825 [physics.ins-det].

[63] J. Aalbers et al. "Solar Neutrino Detection Sensitivity in DARWIN via Electron Scattering". In: (June 2020). arXiv: 2006.03114 [physics.ins-det].

[64] M.J. Berger et al. *XCOM: Photon Cross Section Database (version 1.5)*. 2010. DOI: 10.18434/T48G6X.

[65] C.E. Aalseth et al. "Experimental constraints on a dark matter origin for the DAMA annual modulation effect". In: *Phys. Rev. Lett.* 101 (2008). [Erratum: Phys.Rev.Lett. 102, 109903 (2009)], p. 251301. DOI: 10.1103/PhysRevLett.101.251301. arXiv: 0807.0879 [astro-ph].

[66] T. Aralis et al. “Constraints on dark photons and axionlike particles from the SuperCDMS Soudan experiment”. In: *Phys. Rev. D* 101.5 (2020), p. 052008. DOI: 10.1103/PhysRevD.101.052008. arXiv: 1911.11905 [hep-ex].

[67] D.S. Akerib et al. “First Searches for Axions and Axionlike Particles with the LUX Experiment”. In: *Phys. Rev. Lett.* 118.26 (2017), p. 261301. DOI: 10.1103/PhysRevLett.118.261301. arXiv: 1704.02297 [astro-ph.CO].

[68] Changbo Fu et al. “Limits on Axion Couplings from the First 80 Days of Data of the PandaX-II Experiment”. In: *Phys. Rev. Lett.* 119.18 (2017), p. 181806. DOI: 10.1103/PhysRevLett.119.181806. arXiv: 1707.07921 [hep-ex].

[69] E. Armengaud et al. “Axion searches with the EDELWEISS-II experiment”. In: *JCAP* 11 (2013), p. 067. DOI: 10.1088/1475-7516/2013/11/067. arXiv: 1307.1488 [astro-ph.CO].

[70] M. Agostini et al. “The first search for bosonic super-WIMPs with masses up to 1 MeV/c^2 with GERDA”. In: *Phys. Rev. Lett.* 125.1 (2020), p. 011801. DOI: 10.1103/PhysRevLett.125.011801. arXiv: 2005.14184 [hep-ex].

[71] E. Aprile et al. “First Axion Results from the XENON100 Experiment”. In: *Phys. Rev. D* 90.6 (2014). [Erratum: Phys.Rev.D 95, 029904 (2017)], p. 062009. DOI: 10.1103/PhysRevD.90.062009. arXiv: 1404.1455 [astro-ph.CO].